

Galactic Faraday rotation effect on polarization of 21cm lines from the epoch of reionization

Soma De¹ and Hiroyuki Tashiro²

¹*School of Earth and Space Exploration, Arizona State University, Tempe, AZ 85287, USA*

²*Physics Department, Arizona State University, Tempe, AZ 85287, USA*

Redshifted 21 cm signal from neutral hydrogen is one of the most competitive probes of the epoch of reionization (EoR). Unpolarized 21 cm radiation acquires a certain level of linear polarization during the EoR due to Thomson scattering. This linear polarization, if measured, could probe important information about the EoR. We study the effect of Galactic Faraday rotation (FR) in the detection of polarization of 21 cm radiation. Since the effect of FR is strong due to the large wavelength nature of redshifted 21 cm signal, the initial E-mode signal carried by 21 cm photons is modified in its entirety. We show that a 99% accuracy on rotation measure (RM) data is necessary to recover the initial E-mode signal. We conclude that, given the current status of RM observations, it is not possible to retrieve the initial polarization signal of 21 cm from the EoR. However, we are optimistic that it may be possible from the next generation radio surveys.

I. INTRODUCTION

During the expansion history of our Universe, hydrogen went through different phase transitions. Following nucleosynthesis in the early universe, hydrogen and helium were ionized, and then upon rapid cooling due to expansion, hydrogen became neutral releasing the cosmic microwave background (CMB) radiation. This is known as the epoch of recombination which happened around $z = 1080$ [1]. Past this epoch, the Universe was neutral. Later on high energy photons released by the first stars and quasars again ionized the hydrogen in the inter galactic medium (IGM). This phase is known as the epoch of reionization (EoR). Therefore the expansion history of the universe is encoded in the phases of hydrogen, the most abundant element in the Universe. Probing reionization is a way to learn more about the first stars and first galaxies. The 21 cm line corresponds to the ground state hyperfine transition of atomic hydrogen (see review by Ref. [2]). The condition for detectability of such a signal with respect to background CMB depends on the excitation temperature of the 21 cm transition or the spin temperature. If the spin temperature, T_S deviates from the CMB temperature, a signal may be detectable. This deviation from the background CMB temperature is quantified in terms of the brightness temperature [3] which directly depends on the physical properties of IGM such as density, velocity gradients, gas temperature, level populations and ionization stages.

The statistic of 21 cm brightness temperature fluctuations during the EoR is described by the power spectrum in the Fourier space. This 21 cm power spectrum directly depends on the power of dark matter density fluctuations, baryonic ionization fluctuations and relevant cross terms. Therefore power spectrum plays a crucial role in distinguishing between several models of re ionization dynamics [4, 5]. There have been several papers discussing how the brightness temperature and power spectra of 21 cm could enlighten us on the EoR.

In this paper, we discuss the polarization of the cos-

mological 21 cm signal and Faraday rotation (FR) which plays a major foreground in its detection. Although the major cosmological 21 cm signal is intrinsically unpolarized, as discussed in Ref. [6], polarization in 21 cm radiation could arise from the properties of the sources (e.g. due to Zeeman effect [7]) and primarily Thomson scattering in the EoR. The first polarization sources are very small, although Thomson scattering can create significant level of polarization. The power spectrum of the polarization created through Thomson scattering depends on the re ionization physics such as the number density and the typical size of ionized bubbles. Therefore, the polarization contain complementary information on the EoR to the brightness temperature power spectrum. In particular, Ref. [6] pointed out that the peak scale of polarization power spectrum corresponds to the typical scale of ionized bubbles at the epoch when observed 21 cm radiation is emitted. The detection prospect of any particular type of polarization will depend on the presence of foregrounds. Since its a low-frequency signal, Faraday rotation is a crucial foreground with a definite frequency dependence.

There are several papers for the effect of Galactic Faraday rotation on the measurement of 21 cm signal [8–10]. The Faraday rotation causes the leak of polarized foreground into the estimate of the intrinsically unpolarized signal. Therefore, Galactic Faraday rotation has been studied by using numerical simulation with Galactic Faraday rotation model, in order to estimate a contamination effect of polarized foreground in these papers.

In this paper, we discuss how Galactic FR transforms the initial linear polarization of 21 cm signal originating around the EoR. A calculation on how the linear polarization of CMB is modified as it passes through the Milky Way was done in Ref. [11]. For the case of CMB, although some B-mode polarization is produced due to the Galactic FR effect, the change in the initial E-mode signal is negligible. However, the angle of rotation in the case of 21 cm radiation is large due to the larger wavelength nature of 21 cm photons from EoR. To take into account of

large FR, we build a framework in this paper to calculate the exact polarization spectra under any rotational angle. We then estimate the effect of Galactic Faraday rotation on the initial-E mode polarization coming from EoR.

The organization of the paper is as follows. In Sec. II we discuss the basic principles of Faraday rotation and how it transforms the polarization tensor. In Sec. III, we discuss briefly how the E-mode polarization originated in 21 cm during the EoR. In Sec. IV, we present the Faraday rotation map of our Galaxy and quantify the effect Faraday rotation due to Milky way upon 21 cm E-mode polarization. We conclude our paper by discussing if at all 21 cm polarization may be detected in future experiments and acknowledgments. Throughout this paper, we use cosmological parameters for a flat Λ CDM model: $h = 0.73$ ($H_0 = h \times 100$ km/s/Mpc), $\Omega_c h^2 = 0.104$ and $\Omega_b h^2 = 0.022$.

II. BASICS OF FARADAY ROTATION

If photons emitted at a given redshift, z , with a rest-frame wavelength of 21 cm pass through ionized regions permeated by magnetic fields, the direction of *linear* polarization is rotated by an angle

$$\alpha(\hat{n}) = \lambda_0^2 RM(\hat{n}) = \frac{3}{16\pi^2 e} \lambda_0^2 \int \hat{\tau} \cdot \mathbf{B} \cdot d\mathbf{l}, \quad (1)$$

where \hat{n} is the direction along the line of sight, $\hat{\tau}$ is the differential optical depth, λ_0 is the observed wavelength of the 21 cm radiation at redshift $z = 0$, \mathbf{B} is the ‘‘comoving’’ magnetic field, and $d\mathbf{l}$ is the comoving length element along the photon trajectory. The rotation measure, RM , is a frequency independent quantity in Eq. (1) that describes the strength of Faraday rotation. The observed Stokes parameters upon Faraday rotation angle $\alpha(\hat{n})$ along a chosen direction \hat{n} are given by

$$\begin{pmatrix} Q_{\text{obs}}(\hat{n}) \\ U_{\text{obs}}(\hat{n}) \end{pmatrix} = \begin{pmatrix} \cos 2\alpha(\hat{n}) & \sin 2\alpha(\hat{n}) \\ -\sin 2\alpha(\hat{n}) & \cos 2\alpha(\hat{n}) \end{pmatrix} \begin{pmatrix} Q_i(\hat{n}) \\ U_i(\hat{n}) \end{pmatrix}, \quad (2)$$

where (Q_i, U_i) is the initial Stokes parameters prior to rotation.

The polarization tensor is expressed in terms of the Stokes parameter as

$$P_{\alpha\beta}(\hat{n}) = \begin{pmatrix} Q(\hat{n}) & U(\hat{n}) \\ U(\hat{n}) & -Q(\hat{n}) \end{pmatrix}. \quad (3)$$

The polarization tensor is a symmetric trace-free 2×2 tensor field. Therefore, the polarization tensor can be expanded in terms of tensor spherical harmonics as [12]

$$\mathcal{P}_{ab}(\hat{n}) = \sum_{\ell=2}^{\infty} \sum_{m=-\ell}^{\ell} \left[E_{\ell m} Y_{(\ell m)ab}^E(\hat{n}) + B_{\ell m} Y_{(\ell m)ab}^B(\hat{n}) \right], \quad (4)$$

where $Y_{(\ell m)ab}^E(\hat{n})$ and $Y_{(\ell m)ab}^B(\hat{n})$ are complete sets of basis functions for the E-mode and B-mode components of the polarization [13, 14]. Orthonormality of the basis functions provides E- and B-mode coefficients of polarization as

$$\begin{aligned} E_{\ell m} &= \int d\hat{n} \mathcal{P}_{ab}(\hat{n}) Y_{(\ell m)}^{Eab*}(\hat{n}), \\ B_{\ell m} &= \int d\hat{n} \mathcal{P}_{ab}(\hat{n}) Y_{(\ell m)}^{Bab*}(\hat{n}). \end{aligned} \quad (5)$$

Using Eqs. (2), (3) and (5), we obtain

$$\begin{aligned} E_{\ell m}^{\text{obs}} &= \sum_{\ell'm'} \sum_{LM} \int d\hat{n} Y_{(\ell'm')}^{Eab*}(\hat{n}) Y_{(LM)}(\hat{n}) \\ &\quad \times \left[C_{LM} \left(E_{\ell'm'}^i Y_{(\ell'm')ab}^E(\hat{n}) + B_{\ell'm'}^i Y_{(\ell'm')ab}^B(\hat{n}) \right) \right. \\ &\quad \left. + S_{LM} \left(B_{\ell'm'}^i Y_{(\ell'm')ab}^E(\hat{n}) + E_{\ell'm'}^i Y_{(\ell'm')ab}^B(\hat{n}) \right) \right], \\ B_{\ell m}^{\text{obs}} &= \sum_{\ell'm'} \sum_{LM} \int d\hat{n} Y_{(\ell'm')}^{Bab*}(\hat{n}) Y_{(LM)}(\hat{n}) \\ &\quad \times \left[C_{LM} \left(E_{\ell'm'}^i Y_{(\ell'm')ab}^E(\hat{n}) + B_{\ell'm'}^i Y_{(\ell'm')ab}^B(\hat{n}) \right) \right. \\ &\quad \left. + S_{LM} \left(B_{\ell'm'}^i Y_{(\ell'm')ab}^E(\hat{n}) + E_{\ell'm'}^i Y_{(\ell'm')ab}^B(\hat{n}) \right) \right] \end{aligned} \quad (6)$$

where $C_{\ell m}$ and $S_{\ell m}$ is the spherical harmonic coefficients of $\cos 2\alpha(\hat{n})$ and $\sin 2\alpha(\hat{n})$,

$$\begin{aligned} \cos 2\alpha(\hat{n}) &= \sum_{\ell m} C_{\ell m} Y_{(\ell m)}(\hat{n}), \\ \sin 2\alpha(\hat{n}) &= \sum_{\ell m} S_{\ell m} Y_{(\ell m)}(\hat{n}). \end{aligned} \quad (7)$$

As we discuss later, we consider Thomson scattering in the EoR as a source of the 21 cm polarization. Since Thomson scattering creates the only E-mode, we assume that our initial polarization has $E_{\ell m}^i \neq 0$ and $B_{\ell m}^i = 0$ hereafter.

The integrations in Eq. (6) can be performed as [15]

$$\begin{aligned} &\int d\hat{n} Y_{(\ell'm')ab}^E(\hat{n}) Y_{(\ell'm')}^{Eab*}(\hat{n}) Y_{(LM)}(\hat{n}) \\ &= \int d\hat{n} Y_{(\ell'm')ab}^B(\hat{n}) Y_{(\ell'm')}^{Bab*}(\hat{n}) Y_{(LM)}(\hat{n}) = H_{\ell\ell'}^L \xi_{\ell m \ell' m'}^{LM}, \\ &\int d\hat{n} Y_{(\ell'm')ab}^B(\hat{n}) Y_{(\ell'm')}^{Eab*}(\hat{n}) Y_{(LM)}(\hat{n}) \\ &= \int d\hat{n} Y_{(\ell'm')ab}^E(\hat{n}) Y_{(\ell'm')}^{Bab*}(\hat{n}) Y_{(LM)}(\hat{n}) = 0, \end{aligned} \quad (8)$$

where

$$H_{\ell\ell'}^L \equiv \begin{pmatrix} \ell & \ell' & L \\ 2 & -2 & 0 \end{pmatrix} \begin{pmatrix} \ell & \ell' & L \\ 0 & 0 & 0 \end{pmatrix}^{-1}, \quad (9)$$

in terms of Wigner-3j symbols, and

$$\xi_{\ell m \ell' m'}^{LM} = \int d\hat{n} Y_{(\ell m)}^*(\hat{n}) Y_{(\ell' m')}(\hat{n}) Y_{(LM)}(\hat{n}). \quad (10)$$

The integrations of Eq. (8) are nonzero only for $\ell + \ell' + L = \text{even}$.

Now we can write the observed E-mode and B-mode after Faraday rotation as

$$\begin{aligned} E_{\ell m}^{obs} &= \sum_{\ell' m'} \sum_{LM} C_{LM} \xi_{\ell m \ell' m'}^{LM} H_{\ell \ell'}^L E_{\ell' m'}^i, \\ B_{\ell m}^{obs} &= \sum_{\ell' m'} \sum_{LM} S_{LM} \xi_{\ell m \ell' m'}^{LM} H_{\ell \ell'}^L E_{\ell' m'}^i. \end{aligned} \quad (11)$$

Accordingly, observed E-mode and B-mode autocorrelation can be expressed as

$$\begin{aligned} \langle E_{\ell' m'}^{obs} E_{\ell m}^{obs} \rangle &= \delta_{\ell \ell'} \delta_{m m'} \\ &= \sum_L \left(\frac{2L+1}{4\pi} \right) C_L^{\cos(2\alpha)} \sum_{\ell'} (2\ell'+1) C_{\ell'}^{E,i} (H_{\ell \ell'}^L)^2, \end{aligned} \quad (12)$$

$$\begin{aligned} \langle B_{\ell' m'}^{obs} B_{\ell m}^{obs} \rangle &= \delta_{\ell \ell'} \delta_{m m'} \\ &= \sum_L \left(\frac{2L+1}{4\pi} \right) C_L^{\sin(2\alpha)} \sum_{\ell'} (2\ell'+1) C_{\ell'}^{E,i} (H_{\ell \ell'}^L)^2. \end{aligned} \quad (13)$$

In Eqs. (12) and (13), $C_{\ell}^{E,i}$ indicates the initial E-mode angular power spectrum, and $C_{\ell}^{\sin(2\alpha)}$ and $C_{\ell}^{\cos(2\alpha)}$ are the angular power spectra of $\sin(2\alpha)$ and $\cos(2\alpha)$, respectively.

III. 21 CM E-MODE POLARIZATION FROM THE EOR

Similarly to CMB polarization, 21 cm polarization is generated in the EoR [6]. The fluctuations of emitting neutral hydrogen produce quadrupole temperature anisotropy of free streaming redshifted 21 cm radiation around free electrons in the EoR. Thomson scattering with this quadrupole anisotropy radiation generates a linear polarization. The generated 21 cm polarization can be decomposed into E- and B-modes [13, 14]. Since the fluctuations of neutral hydrogen are due to the baryon and ionization fraction fluctuations, the generated polarization is only E-mode, due to the parity invariance.

Following the total angular momentum representation of CMB polarization [16], the E-mode polarization power spectrum of the redshifted 21 cm fluctuations can be expressed as [6]

$$\begin{aligned} C_{\ell}^{E,i}(\nu) &= \frac{2}{\pi} \int k^2 dk \left[\bar{x}_H^2 P_{\delta}(k) (\delta \Delta_{\ell}^E(k, \nu))^2 \right. \\ &\quad \left. + P_x(k) ({}_x \Delta_{\ell}^E(k, \nu))^2 \right], \end{aligned} \quad (14)$$

where \bar{x}_H is the average ionization fraction, $P_{\delta}(k)$ is the baryonic power spectrum and $P_x(k)$ is the ionization fraction power spectrum.

In Eq. (14), $\delta \Delta_{\ell}^E(k, \nu)$ and ${}_x \Delta_{\ell}^E(k, \nu)$ are the transfer functions of the quadrupole component for the baryon

fluctuations and ionization fraction fluctuations, respectively,

$$\begin{aligned} \delta \Delta_{\ell}^E(k, \nu) &= \frac{3}{4} \sqrt{\frac{(\ell+2)!}{(\ell-2)!}} \int_0^{\eta_R} d\eta \\ &\quad \times \frac{g(\eta)}{\eta^2 k^2} j_{\ell}(k\eta) [j_2(k(\eta_E - \eta)) - j_2''(k(\eta_E - \eta))], \end{aligned} \quad (15)$$

$${}_x \Delta_{\ell}^E(k, \nu) = \frac{3}{4} \sqrt{\frac{(\ell+2)!}{(\ell-2)!}} \int_0^{\eta_R} d\eta \frac{g(\eta)}{\eta^2 k^2} j_{\ell}(k\eta) j_2[k(\eta_E - \eta)], \quad (16)$$

where η_E is the conformal time at the emission redshift.

For the case of $z_E \sim z_r$, the polarization due to ionization fraction fluctuations dominates the one due to the baryon fluctuations [6]. Therefore, we take into account only P_x contributions hereafter.

The power spectrum P_x depends on the reionization model. We calculate P_x following the way of [6], in which, although they considered only Poisson fluctuations, P_x is evaluated robustly.

First, we model the average ionization fraction to be a function of redshift as used in CAMB [17]

$$\bar{x}_e(z) = \frac{1}{2} \left[1 + \tanh \left(\frac{2(1+z_r)^{3/2} - (1+z)^{3/2}}{3\Delta z(1+z_r)^{1/2}} \right) \right], \quad (17)$$

with $\Delta z \sim 0.5$.

Around the end of reionization, the bubble starts to overlap [18]. Therefore, the mean distance between ionized bubbles corresponds to the characteristic size of the bubbles. We define the averaged number density of ionized bubbles at z_r as

$$\bar{n} = \frac{3}{4\pi} R_r^{-3}, \quad (18)$$

where R_e is the characteristic size of the bubbles at z_r . During the reionization process, the characteristic scale of ionized bubbles starts to grow from a scale smaller than R_r , grows with time and finally reach R_r . To take into account the growth of the characteristic scale, we simply assume that the average bubble density is constant and the characteristic scale of bubbles, $R(z)$, evolves to satisfy

$$\bar{x}_e(z) = \frac{4\pi}{3} \bar{n} R(z)^3. \quad (19)$$

Assuming that ionized bubbles are point-like objects, the two-point correlation function for Poisson contribution is given by

$$\langle \delta x_p(\mathbf{r}_1) \delta x_p(\mathbf{r}_2) \rangle = \frac{1}{\bar{n}(\mathbf{r}_1)} \delta^{(3)}(\mathbf{r}_1 - \mathbf{r}_2), \quad (20)$$

where δx_p is the fluctuations of the ionization fraction due to the point-like objects and we assume that the inside of ionized bubbles are totally ionized. However,

actual ionized bubbles have a finite size R . In order to consider the finite size effect, we take the convolution with a window function,

$$\delta x(\mathbf{r}_1) = \int d^3 \mathbf{r}_2 W_R(|\mathbf{r}_1 - \mathbf{r}_2|) \delta x_p(\mathbf{r}_2), \quad (21)$$

where we adopt a Gaussian window function with the window size R ,

$$W_R(r) = \frac{e^{-r^2/2R^2}}{\sqrt{(2\pi)^3 R^3}}. \quad (22)$$

Therefore, we can write the two-point correlation function of the ionized fraction as

$$\begin{aligned} \langle \delta x(\mathbf{k}_1) \delta x^*(\mathbf{k}_2) \rangle &= \int d^3 \mathbf{r}_1 d^3 \mathbf{r}_2 e^{i\mathbf{k}_1 \cdot \mathbf{r}_1} e^{-i\mathbf{k}_2 \cdot \mathbf{r}_2} \\ &\times \int d^3 \mathbf{y}_1 d^3 \mathbf{y}_2 \frac{e^{-|\mathbf{r}_1 - \mathbf{y}_1|^2/2R^2}}{\sqrt{(2\pi)^3 R^3}} \frac{e^{-|\mathbf{r}_2 - \mathbf{y}_2|^2/2R^2}}{\sqrt{(2\pi)^3 R^3}} \\ &\times \langle \delta x_p(\mathbf{y}_1) \delta x_p(\mathbf{y}_2) \rangle. \end{aligned} \quad (23)$$

Defining the power spectrum of the ionization fraction $P_x(k)$ as $\langle \delta x(\mathbf{k}_1) \delta x^*(\mathbf{k}_2) \rangle = (2\pi)^3 \delta^{(3)}(\mathbf{k}_1 - \mathbf{k}_2) P_x(k_1)$, we obtain the power spectrum,

$$P_x(k) = \frac{1}{\bar{n}} e^{-k^2 R^2}. \quad (24)$$

Accordingly, the peak scale of the power spectrum corresponds to the typical scale of ionized bubbles in our model.

IV. EFFECT OF MILKY WAY ON LINEAR POLARIZATION OF 21 CM

In this section, we investigate how the linear polarization of 21 cm signal described in Sec. III gets modified as it propagates through the Galaxy. In our calculation, we assume that, during the EoR, only E-mode polarization was created which then gets transformed into E-mode and B-mode due to the Galactic Faraday rotation according to the equations described in Sec. II.

Faraday rotation in Milky Way is measured by observing extragalactic polarized radio sources. Oppermann et al. have released publicly available rotation measure (RM) map of Milky Way [19]. They have reconstructed the RM maps based on the RM catalog of the NRAO VLA Sky Survey [20] with several other catalogs. In this paper, we adopt their public data as the Galactic RM map. The RM and its uncertainty are strongest along the Galactic disk. Therefore, the Galactic disk is the source of highest amount of foreground. We choose to remove this area for our calculations, by adopting Planck's mask 30 GHz [21].

In Fig. 1, we present the angle of rotation of linear polarization of 21 cm radiation based on the data of Ref. [19] as it passes through the Galaxy. Due to the rest-frame

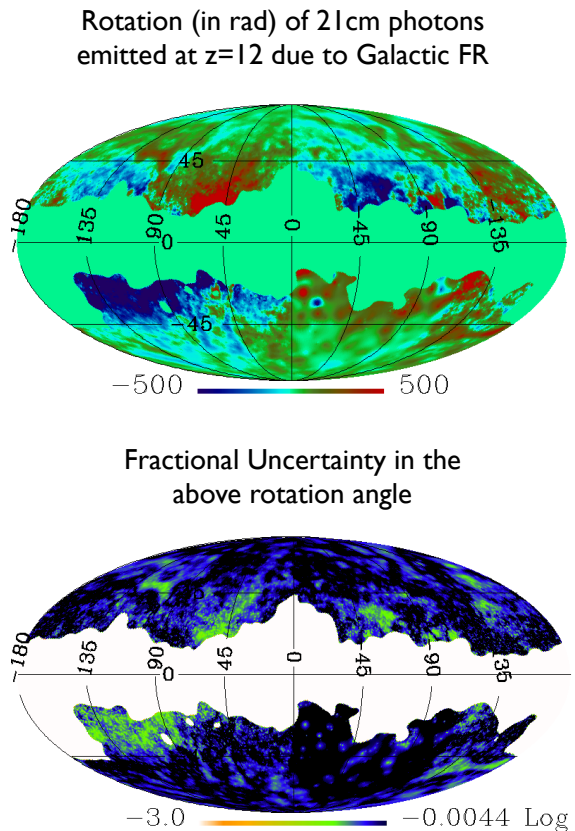


FIG. 1: The Faraday rotation angle in radian of the rest frame 21 cm photons from $z = 12$ (top panel) and the fractional uncertainty in the rotation angle (bottom panel).

low frequency of these photons, the rotation angle is high. The top panel of Fig. 1 shows the rotation angle in radian. The bottom panel indicates fractional uncertainty in the rotation angle. From Sec. II, Faraday rotation angle is proportional to square of the observed wavelength. Therefore rotation angle increases as $(1+z)^2$ with redshift. For the particular case of Fig. 1, we assume that 21 cm radiation was emitted at $z = 12$. From the magnitude of the rotation angle it is evident that there are regimes with angle of rotation being significantly larger than 2π radian. This creates a degeneracy in the rotation angle or the RM along the line of sight. In order to reconstruct the initial polarization, one should therefore be careful since along many lines of sight the linear polarization may have been rotated by an angle larger than 2π .

In Fig. 2, we present cosine and sine of twice the angle of rotation due to the Galactic magnetic field. We chose to plot twice the angle of rotation following the equations in Sec. II which involves a trigonometric factor of 2α where α is the Faraday rotation angle. The top panel of Fig. 2 indicates full strength of Faraday rotation spanning the entire range between -1 and 1 . The mid panel of Fig. 2 shows cosine and sine of twice the angle of

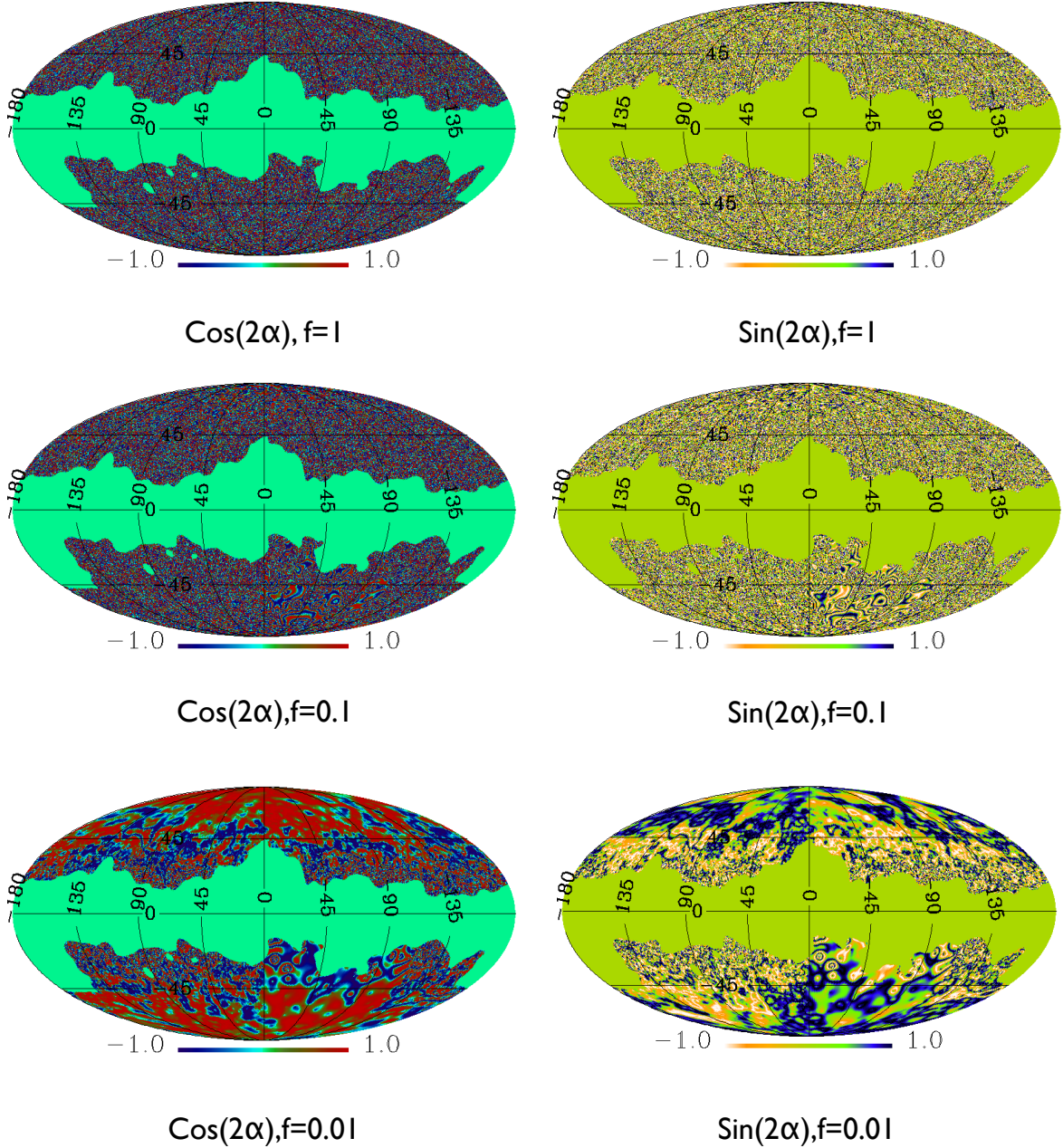


FIG. 2: Faraday rotation maps. Top panel shows Cosine and Sine of twice the angle of rotation as 21 cm photons emitted at $z=12$ pass through the galaxy. Mid and bottom panels respectively indicate where RM is respectively 0.1 and 0.01 of the actual value.

Faraday rotation when only 10% RM is used. We parameterize the chosen RM strength by a factor $f = 0.1$. The bottom panel displays the rotation angle when only 1% RM was used or $f = 0.01$. It is useful to investigate maps of $\sin(2f\alpha)$ or $\cos(2f\alpha)$ for the following reason. If the Galactic RM is known over all sky or over certain patches of the sky with sufficient accuracy (with less than 1% error), then the information about the initial E-mode

polarization of 21 cm photons can be recovered. The polarization information is completely lost due to the large rotation suffered by 21 cm photons emitted at $z \sim z_r$ as it passes through our Galaxy. Therefore, if Galactic RM is known with sufficient accuracy along several lines of sight and RM is comparatively low along those lines of sight, the initial linear polarization of 21 cm photons could be recovered along those lines. This conclusion is based on

the assumption that there is no other foreground.

We construct $C_\ell^{\sin(2\alpha)}$ and $C_\ell^{\cos(\alpha)}$ from the observed FR map. The Galactic FR map has a strong latitude dependence. We simply define the rotation angular spectrum as

$$C_\ell^{\alpha\alpha} \equiv (2\ell + 1)^{-1} \sum_m \alpha_{\ell m}^{\text{map}*} \alpha_{\ell m}^{\text{map}}. \quad (25)$$

Similarly, we obtain

$$C_\ell^{\sin(2\alpha)} = (2\ell + 1)^{-1} \sum_m (\sin 2\alpha)_{\ell m}^{\text{map}*} (\sin 2\alpha)_{\ell m}^{\text{map}},$$

$$C_\ell^{\cos(2\alpha)} = (2\ell + 1)^{-1} \sum_m (\cos 2\alpha)_{\ell m}^{\text{map}*} (\cos 2\alpha)_{\ell m}^{\text{map}} \quad (26)$$

We construct $C_\ell^{\sin(2\alpha)}$ and $C_\ell^{\cos(\alpha)}$ from the observed FR map. In Fig. 3, we present the power spectra $\ell(\ell + 1)C_\ell^{\text{RM}}/2\pi$ of $\sin(2f\alpha)$ and $\cos(2f\alpha)$ where α is the rotation in linear polarization of rest-frame 21 cm photons emitted at redshift $z = 12$. The solid, dotted and dashed lines respectively indicate $f = 1, 0.1, 0.01$. Each of these power spectra are calculated upon removing the Galactic disk by Planck mask cut at 70 GHz which corresponds to a $f_{\text{sky}} = 0.7$. We notice from Fig. 3 that corresponding to $f = 0.01$, both sine and cosine of $2f\alpha$ reach almost a scale-invariant shapes. This scale invariance breaks down with $\ell > 200$ corresponding to around 0.6 degree. For higher values of f , we find that the power due to $\sin(2f\alpha)$ or $\cos(2f\alpha)$ to be $\sim \ell^2$ implying a white-noise like power in C_ℓ . We find that, upon reducing f upto 0.001, the power in $\sin(2f\alpha)$ starts to resemble RM power spectra in [11] still remaining largely scale-invariant. At this point, power in $\cos(2f\alpha)$ becomes insignificant. So far we have explored quantitative nature of Faraday rotation angle due to our Galaxy on 21 cm polarization. Next, we investigate the effect of FR in E-mode polarization level originating from the EoR.

In Fig. 4, we present E-mode polarization of 21 cm radiation coming from the EoR. On the top panel, the initial E-mode angular power spectra are by solid lines. Setting that the observation redshift corresponds to the reionization redshift, $z = z_r$, we choose two redshifts, $z = 8, 12$ respectively indicated by black and red solid lines. In the top panel, we choose a bubble radius, $r = 70$ Mpc. With dotted, dashed and dot-dashed lines we present the transformed E-mode polarization after FR due to the Milky way with different choices of RM strengths. Dotted lines show when full strength of FR was applied. Dashed and dot-dashed lines respectively indicate when only 10 and 1% RM was used to transform the initial E-modes according to Eq. (12). The bottom panel of Fig. 4 shows how the initial E-mode polarization power transforms under FR when different bubble radii were chosen. The initial polarization is chosen to have formed at $z = 8$. The black and green solid lines are chosen respectively to represent bubble radii of 10 and 120 Mpc respectively. Similar to the top panel, the dotted, dashed and dot-dashed lines represent 100, 10 and 1% RM strength.

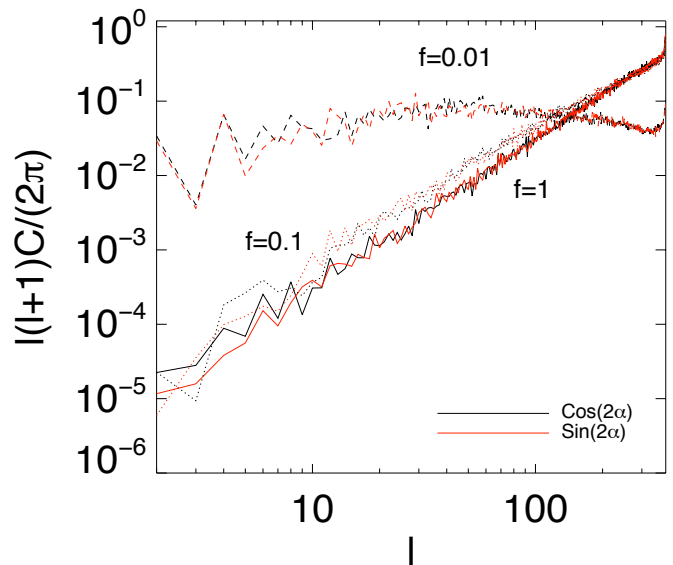


FIG. 3: Power spectra of the sine and cosine of the rotation angle corresponding to Faraday rotation of 21 cm photons emitted and polarized at $z = 12$ with different levels of RM strength.

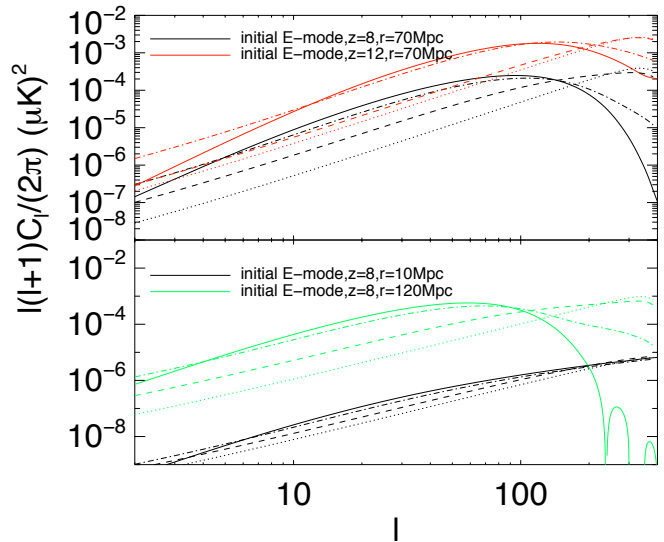


FIG. 4: E-mode polarization spectra of 21 cm photons around the EoR. The solid lines represent the initial E-mode power at the indicated redshifts. The dotted, dashed and dot-dashed lines show E-modes generated when RM is 100, 10 and 1 percent of the actual magnitude.

Our conclusion from Fig. 4 is that with $f = 0.01$ (with 1% of RM strength) one may be able to reconstruct the initial E-mode spectra (upto $\ell \sim 100$), especially around the peak scale, in the absence of any other foreground. The peak scale corresponds to the typical size of ionized bubbles. Therefore, we can access the evolution of the ionized bubble size with $f = 0.01$.

In Fig. 5, we present how the E-mode polarization of

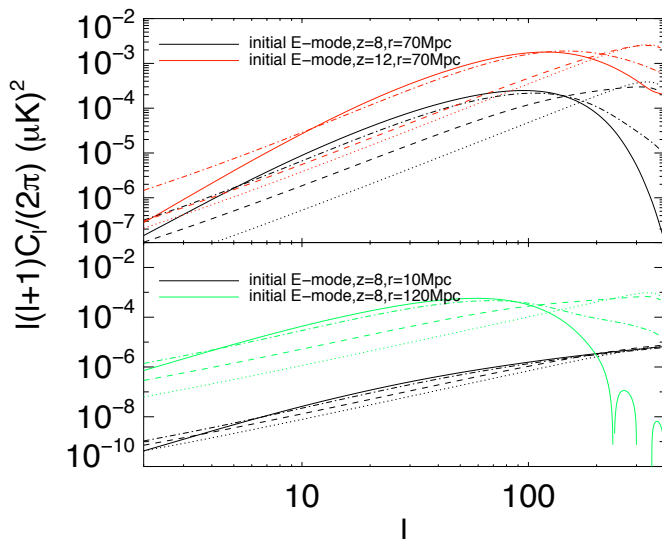


FIG. 5: B-mode polarization spectra of 21 cm photons after they pass through the Milky way. Solid lines are for the initial E-mode at the indicated redshifts. The dotted, dashed and dot-dashed lines represent B-modes generated when RM is 100,10 and 1 percent of the actual strength.

21 cm radiation coming from the EoR transforms into B-modes due to FR from the Milky way. On the top panel, the initial E-mode angular power spectra for $z = 8$ and 12 are indicated by black and red solid lines, respectively. We choose $r = 70$ Mpc for a bubble radius. With dotted, dashed and dot-dashed lines, we represent the transformed B-mode polarization after FR due to the Milky way. Dotted lines indicate when the full strength of RM was applied. Dashed and dot-dashed lines respectively are for the cases where only 10 and 1% RM was used to transform the initial E-modes into B-modes according to Eq. (13). The bottom panel of Fig. 5 shows how the initial E-mode polarization power spectrum transforms into B-modes under FR for different bubble radius. The initial polarization is chosen to have formed at $z = 8$ with $z_r = 8$. The black and green solid lines are chosen respectively to present bubble radii of 10 and 120 Mpc. Similar to the top panel the dotted, dashed and dot-dashed lines indicate 100,10 and 1% FR strength. Similar to transformation of E-modes into E-modes (as described in Fig. 4), we find that B-modes tend to replicate the initial E-modes if $f < 0.01$ upto $\ell < 200$.

We investigate if there is a smooth area on the Galactic sky where the amount of RM is small and also known with 99% accuracy (see Fig. 2). Given the current status of FR data, we find that there are only a few scattered lines of sights with such desired accuracy and therefore construction of a smooth map is not possible among those points.

V. SUMMARY AND OUTLOOK

The goal of this paper is to examine to what extent FR due to the Galaxy affects the initial E-mode polarization of the 21 cm radiation and investigate if it is possible at all to recover the initial signal given the current accuracy of FR data. 21 cm radiation usually unpolarized and picks up a linear E-mode polarization during the EoR from Thomson scattering. In our calculation we investigate how this linear polarization transform under the Galactic FR.

We exclude any other additional contributions to RM outside of our Galaxy. This additional contribution could come from the IGM with large scale magnetic field of a few nG over a large path length. There could also be contribution due to locally strong magnetic field, for example, due to a quasar along the line of sight. In our paper we exclude such effects and consider the effect of only the large scale magnetic field due to the Milky way on the E-mode polarization of 21 cm radiation from the EoR.

From Fig. 2, we notice that given the full strength of FR due to only our Galaxy, angle of rotation of the polarization corresponding to 21 cm radiation coming from the EoR gets rotated by a large angular range (larger than 2π). This destroys the initial signal entirely. From the bottom panel of the same Figure, we see that some signal may be recovered if the FR data is known within 99% accuracy. In Fig. 1, we present the uncertainty in the current FR map from Oppermann dataset. We find that given this existing FR catalog based on the extragalactic polarized radio sources, there are only a few scattered points where the desired accuracy to recover the initial E-mode signal is achieved. Construction of a smooth map where the Galactic RM is known with 99% is not possible given the current status of observations. Since the EoR redshift range is not precisely determined, one may choose a lower redshift (for example $z = 6$) reducing the amount of rotation. This choice, however, reduces the initial E-mode signal [6]. Therefore we conclude that given the current status of extra-galactic dataset mapping out the Faraday sky, it is not possible to reconstruct the initial E-mode polarization of the 21 cm signal originating from the EoR.

However, Low Frequency Array (LOFAR) [22] and the next generation of radio survey, Square Kilometre Array (SKA) [23], is expected to improve Galactic RM data by their pulsar surveys [24]. Such improvement may allow us to construct a smooth map within 99% accuracy and access the polarization signal of 21 cm radiation from the EoR.

Acknowledgments

We are grateful to Niels Oppermann and collaborators [19] for making their rotation measure maps publicly available at [25]. Some of the results in this paper

have been derived using the HEALPix [26, 27] package. We thank Levon Pogosian and Tanmay Vachaspati for an earlier collaboration which was a motivation for this work. We also thank Yin-Zhe Ma and Andrew Long for

discussions and helpful comments. SD is supported by a NASA Astrophysics Theory Grant NNX11AD31G and HT is supported by the DOE at ASU.

-
- [1] W. Hu, ArXiv e-prints (2008), [0802.3688](#).
- [2] J. R. Pritchard and A. Loeb, Reports on Progress in Physics **75**, 086901 (2012), [1109.6012](#).
- [3] M. F. Morales and J. S. B. Wyithe, Annual Review of Astron and Astrophys **48**, 127 (2010), [0910.3010](#).
- [4] K. W. Masui, E. R. Switzer, N. Banavar, K. Bandura, C. Blake, L.-M. Calin, T.-C. Chang, X. Chen, Y.-C. Li, Y.-W. Liao, A. Natarajan, U.-L. Pen, *et al.*, Astrophys. J. Lett. **763**, L20, L20 (2013), [1208.0331](#).
- [5] E. D. Kovetz and M. Kamionkowski, Phys. Rev. Lett. **110**(17), 171301, 171301 (2013), [1211.4610](#).
- [6] D. Babich and A. Loeb, Astrophys. J. **635**, 1 (2005), [arXiv:astro-ph/0505358](#).
- [7] A. Cooray and S. R. Furlanetto, Monthly Notices of the Royal Astronomical Society **359**, L47 (2005), [arXiv:astro-ph/0408314](#).
- [8] V. Jelic, S. Zaroubi, P. Labropoulos, G. Bernardi, A. G. de Bruyn and L. V. E. Koopmans, Monthly Notices of the Royal Astronomical Society, **409**, 1647, 2010
- [9] P. M. Geil, B. M. Gaensler, J. Stuart and B. Wyithe, Monthly Notices of the Royal Astronomical Society, **418**, 516, 2011
- [10] D. F. Moore, J. E. Aguirre, A. R. Parsons, D. C. Jacobs and J. C. Pober, Astrophys. J., **769:154**, , 2013 June 1 (11pp) [[arXiv:1302.0876](#) [astro-ph.CO]].
- [11] S. De, L. Pogosian, and T. Vachaspati, ArXiv e-prints (2013), [1305.7225](#).
- [12] M. Kamionkowski, Phys. Rev. Lett. **102**, 111302 (2009) [[arXiv:0810.1286](#) [astro-ph]].
- [13] M. Kamionkowski, A. Kosowsky and A. Stebbins, Phys. Rev. Lett. **78**, 2058 (1997) [[astro-ph/9609132](#)].
- [14] M. Zaldarriaga and U. Seljak, Phys. Rev. D **55**, 1830 (1997) [[astro-ph/9609170](#)].
- [15] W. Hu, Phys. Rev. D **62**, 043007 (2000) [[astro-ph/0001303](#)].
- [16] W. Hu and M. J. White, Phys. Rev. D **56**, 596 (1997) [[astro-ph/9702170](#)].
- [17] A. Lewis, A. Challinor and A. Lasenby, Astrophys. J. **538**, 473 (2000) [[arXiv:astro-ph/9911177](#)].
- [18] J. S. B. Wyithe and A. Loeb, Nature, **432**, 194 (2004) [[astro-ph/0409412](#)].
- [19] N. Oppermann, H. Junklewitz, G. Robbers, M. R. Bell, T. A. Ensslin, A. Bonafede, R. Braun and J. C. Brown *et al.*, [arXiv:1111.6186](#) [astro-ph.GA].
- [20] J. J. Condon, W. D. Cotton, E. W. Greisen, Q. F. Yin, R. A. Perley, G. B. Taylor and J. J. Broderick, Astron. J. **115**, 1693 (1998).
- [21] <http://pla.esac.esa.int/pla/aio/planckProducts.html>
- [22] <http://www.lofar.org/>
- [23] <http://www.skatelescope.org/>
- [24] R. Beck, AIP Conf. Proc., **1381**, 117 (2011)
- [25] <http://www.mpa-garching.mpg.de/ift/faraday/>
- [26] <http://healpix.jpl.nasa.gov>
- [27] K. M. Gorski, E. Hivon, A. J. Banday, B. D. Wandelt, F. K. Hansen, M. Reinecke and M. Bartelman, Astrophys. J. **622**, 759 (2005) [[astro-ph/0409513](#)].